Triply differential measurements of single ionization of argon by 1-keV positron and electron impact

J. Gavin,[1] O. G. de Lucio,[2,*] and R. D. DuBois[3]
[1]*The University of Arkansas at Monticello, Monticello, Arkansas 71656, USA*
[2]*Instituto de Física, Universidad Nacional Autónoma de México, Apartado Postal 20, 364 01000 México DF, Mexico*
[3]*Department of Physics, Missouri University of Science and Technology, Rolla, Missouri 65409, USA*
(Received 30 March 2017; published 14 June 2017)

By establishing coincidences between target ions and scattered projectiles, and coincidences between target ions, scattered projectiles, and ejected electrons, triply differential cross-section (TDCS) information was generated in terms of projectile energy loss and scattering angles for interactions between 1-keV positrons and electrons and Ar atoms. The conversion of the raw experimental information to the TDCS is discussed. The single-ionization TDCS exhibits two distinguishable regions (lobes) where binary and recoil interactions can be described by two peaks. A comparison of the positron and electron impact data shows that the relative intensity of both binary and recoil interactions decreases exponentially as a function of the momentum transfer and is larger when ionization is induced by positron impact, when compared with electron impact.

DOI: 10.1103/PhysRevA.95.062703

I. INTRODUCTION

Ionization by electron impact has been exhaustively studied over many decades, with a special interest in describing inelastic interactions. These studies usually have focused on measurements of ionization probabilities and the kinematics involved during and after the collision process. See, for example, Refs. [1–3]. More recently ionization by antiparticle impact (positron and antiproton) has been a trending subject for both theoretical and experimental physicists. For positrons, in many of the recent experimental studies it has been a common practice to use noble gas atoms as targets [4], where individual interactions between the involved particles can be more easily described by theory. The goal of such experiments is to provide accurate information on similarities or differences between particle-matter and antiparticle-matter interactions, as well as to isolate and study certain channels and processes, in order to test theoretical models in more detail. The importance of performing such tests arises from the fact that, while first-order perturbation theories employed to describe such interactions predict identical total and differential cross sections for high-energy particle and antiparticle impact; more sophisticated approximations show differences in the differential electron emission measured as a function of the momentum transfer [5–7]. For example, binary electron emission (produced by interactions where the other bound electrons and target nucleus act as spectators) is expected to be enhanced (decreased) for positron (electron) impact, while the recoil emission (due to interactions where the ejected electron also interacts with the target nucleus as it leaves) is predicted to show opposite effects. Depending on the sign of the charge, the directions of the binary and recoil lobes are also predicted to shift with respect to the momentum-transfer direction [8].

Results presented here complement a series of studies performed at the Missouri University of Science and Technology that allow a direct comparison of positron and electron impact. Here, fully kinematic data have been measured for a range of electron emission angles and energies for 1-keV positron and electron impact. By using identical experimental conditions for both positron and electron impact, uncertainties associated with different apparatuses and techniques are minimized. Also, using the number of ionization events recorded, the positron and electron impact data can be normalized to each other. Thus, after decades, the predicted differences arising from the sign of the projectile charge can finally be tested. This paper (and our previous studies [9–11]) also helps to establish how atomic interactions such as electron exchange, polarization effects, and postcollision interactions contribute, thus allowing for a better understanding of positron interactions, which is an important subject in a variety of fields, e.g., production of antihydrogen and derived fundamental studies of QED, *CPT*, and gravitational forces on antimatter [12], applications such as personal electronic transfer imaging in medicine [13–15], as well as characterization of materials by techniques such as angular correlation of annihilation radiation [16–18]. To provide a more detailed idea on the growing importance of such an area of study, the reader is referred to Ref. [19], where several examples of applications of positrons in different areas can be found.

II. EXPERIMENTAL

The positron beam was produced using a ^{22}Na radioactive source with a tungsten moderator, and was delivered to the target by means of an electrostatic transport system. For the electron beam, an electron gun plus a 90° deflector were inserted into the positron beamline, such that the deflected electron beam entered the scattering chamber via the same input aperture and trajectory used for positron impact. Figure 1 shows a schematic of the interaction region and the various detectors. Ions created by the collision of the projectile and an effusive gas jet target were extracted by a weak electric field produced by plates above and below the interaction region and detected by a channeltron. Time-of-flight (TOF) techniques were used to distinguish their charge states and masses. After the interaction region the projectile scattering angles and energies were measured using an electrostatic energy analyzer and a channelplate position sensitive detector (projectile PSD). Electrons ejected from the target were recorded as a function

*Corresponding author: dododrillo@yahoo.com

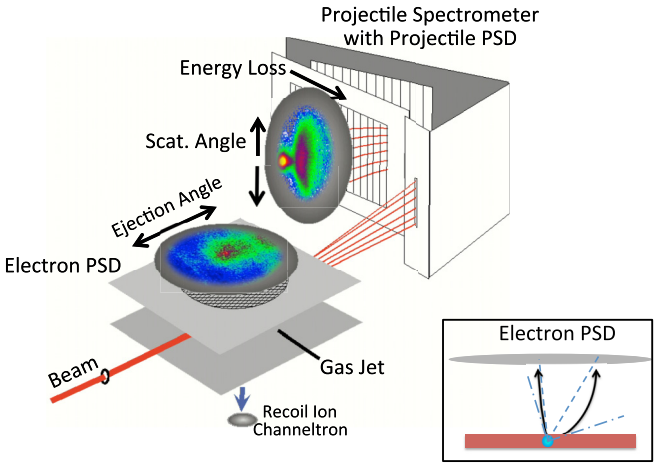

FIG. 1. Schematic of interaction region and detectors. The arrows indicate the electron ejection angles and the projectile scattering angles and energy loss respective to the noninteracting beam (the localized dot seen on the projectile detector). In the inset a sideview of the extraction region is shown, where the emission angle (dot-dashed lines) and the geometric angle (dashed lines) are indicated.

of angle using a second PSD positioned above the interaction region. Coincidences between target ions, scattered projectiles, and ejected electrons provided triply differential cross-section (TDCS) information that could be associated either for the scattered projectile or for the ejected electron channel. In both cases, the position sensitive detectors provided these data for a range of scattering and emission angles and energy losses. It is important to note that the TDCS data obtained for the scattered projectile channel are for all ejected electrons of a given energy ejected between 30 and 150° with respect to the beam direction. Thus, the scattered projectile TDCS represents the total intensity of the portions of the binary and recoil electron emission lobes that we can observe whereas the ejected electron TDCS data show the structure of these lobes. Here we concentrate only on the ejected electron TDCS data.

As described in previous publications [9–11,20] two-dimensional (2D) spectra are generated for scattered projectiles, where one axis corresponds to the projectile scattering angles and the other corresponds to the energy loss. Forward scattered projectiles were limited to a horizontal scattering range ($\varphi_{\rm scat}$ angle) of $0^\circ \pm 2.4^\circ$ by a slit at the entrance to the energy analyzer and to vertical scattering angles ($\theta_{\rm scat}$) between $\pm 7^\circ$. For the present paper, the spectrometer voltages were adjusted to select energy losses less than ~150 eV. No direct energy analysis of the ejected electrons was used. Instead, for single ionization their energies, ε, were determined by using coincidences with projectiles that suffered a known energy loss. For our geometry negative (positive) scattering angles imply that the projectile is scattered vertically downwards (upward). Because of the location of the electron detector, only the "upward" emitted electrons should be recorded. Thus, the correlated downward (upward) scattered projectiles and upward emitted target electrons are a direct indication of binary (recoil) events since the scattered projectile and ejected electron are detected in opposite (same) hemispheres.

III. DATA ANALYSIS AND RESULTS

Experimental results were recorded in list mode files. Such files were re-sorted afterwards using double coincidences to generate one-dimensional TOF spectra to distinguish between different degrees of ionization and random versus real events and triple coincidences to generate 2D spectra for scattered projectiles (scattered projectile intensity as a function of scattering angle and energy loss) and for the ejected electrons (electron intensity as a function of theta and phi emission angles). This is done for both the real+random and the random events in order to perform a background subtraction and generate spectra with only true coincidences. Most of the scattered projectile 2D background spectrum is associated with the nonscattered beam (the localized dot at the center left of the projectile detector), thus unequivocally establishing the zero degree scattering angle and zero energy loss.

By setting conditions on the projectile scattering angle and energy loss, 2D spectra for electron emission for different values of momentum transfer are generated. A "slice" along the direction of the beam (geometric emission angles of 30–150° and $+/-20^\circ$ along and perpendicular to the beam direction) was then taken to provide the TDCS for "in-plane" electron emission for both binary and recoil interactions. To improve the statistics, along the beam direction the data were binned into 5-pixel-wide bins corresponding to geometric emission angles of ~3° at the detector edge and ~9° at its center. Additional experimental details and considerations can be found in Refs. [9–11,20].

During the early stages of this work, experimental evidence showed that the electric field used to extract the target ions could significantly modify both the directions and acceptance ranges of the recorded ejected electrons. Very low ejected electron energies could even be turned around by the electric field. In order to minimize this problem, the extraction field was kept as low as possible (for this work a field of 1.2 V/cm was used). At the time, a combination of SIMION simulations and a detailed computer model of the interaction volume and fields indicated that such problems were minimal for emission energies above a few eV. On the other hand, to achieve enough statistics for positron impact, a relatively large beam diameter (6 mm) was used. The large beam diameter combined with the spectrometer energy resolution near 1 keV means that a broad range of energy losses, hence, emission energies, contributes for any particular energy-loss bin used to generate the TDCS. This introduces a range of electric-field effects and uncertainties in determining which emission angles and energies contributed at each emitted electron observation position. Thus, at that time only a limited comparison of triply differential yields obtained for positron and electron impact was possible [21].

However, as described in a recent publication [20], by using a detailed SIMION simulation of electron emission and detection in electric fields as used in our experiment, we are now able to convert our measured yields to triply differential cross sections. How this is done is described below.

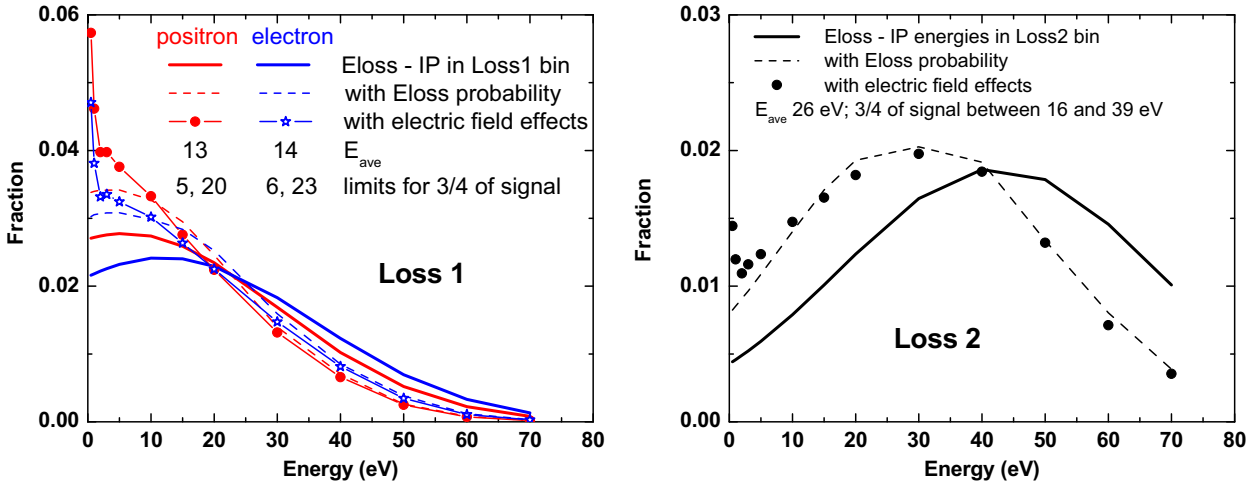

FIG. 2. Calibration of the energies associated with the energy-loss 1 window (left) for both positron and electron projectiles and loss 2 window (right) for both projectiles. Solid curves correspond to a normalized convolution of the beam profile and window bin size, dashed curves consider the electron loss probabilities, and points include results from SIMION simulations, taking into account how the electric fields present in the interaction region influence the ejected electron detection probabilities. The area under each distribution has been normalized to unity.

A. Determination of experimental parameters

1. Energy-loss (ejected electron energies) calibration

As mentioned, because of the limited positron beam intensity that was available, to achieve sufficient statistics, a large diameter beam was used. Plus, a range of energy losses was binned for the data presented here. The large diameter beam meant that, on the projectile PSD, the noninteracting beam produced an intensity distribution roughly 6 mm in diameter. SIMION simulations showed that, independent of scattering angle, the spectrometer employed focuses identical energy projectiles to the same horizontal channel of our projectile position sensitive detector. This confirmed that our observed near-Gaussian horizontal beam profile represents a difference in beam intensities, rather than differences in beam energy, i.e., each horizontal channel in this profile corresponds to the full beam energy (including of course the initial energy spread from the source).

The large diameter beam also meant that at each energy-loss channel on the projectile PSD, a range of projectile energy losses can contribute. This is because any projectiles originally on the far side of the beam that have interacted and are observed at a particular energy-loss channel have suffered a larger energy loss than similar projectiles that were originally on the near side of the beam. Thus, for each energy-loss channel it is necessary to determine which energy losses contribute and how much of the observed signal is associated with each energy loss. This was done by starting at the farthest part of the beam profile and first determining the relative amount of the total Gaussian beam intensity convoluted with the relative amount of the "inherent" source intensity. For the "inherent" source intensity an exponential with half width of 1.5 eV was used. Then, the resulting relative intensity was multiplied by the energy loss determined from the channel separation between this point in the beam intensity profile and the energy-loss channel in question times the energy/channel for the spectrometer voltages used. This procedure was then repeated for the next closest channel of the beam profile, and so on, until the entire beam profile had been included. For energy-loss channels close to the beam, portions of the beam profile were shown to yield energy losses less than the ionization potential. These portions were not included. After including all contributions for a particular energy-loss bin, the weighted energy losses were summed and divided by the entire beam profile intensity to determine the average energy loss and the range of energy losses for this bin. Subtracting the ionization potential yields projectile energy distributions contributing to a specific energy-loss bin.

As shown in Fig. 2, this yielded a Gaussian energy-loss profile with truncated wings because a portion of the beam was either restricted from contributing or due to the finite bin width used. Normalized to unity, the solid curves show the distribution of energies, i.e., the energy loss minus the ionization potential, accepted in each case studied. These truncated Gaussian profiles have mean energies of ~ 21 and 36 eV but because of the large range of energy losses these distributions have to be modified by the energy-loss probabilities. The energy-loss probabilities were obtained by projecting our measured 2D projectile spectra along the energy-loss axis. The results, shown by the dashed curves, have lower mean energies of 16 eV (positron) and 18 eV (electron) for the loss 1 bin and 26 eV for the loss 2 bin. Although these energies mean that both $3s$ and $3p$ ionization is possible, statistics and ionization probabilities imply that the measured TDCSs are primarily associated with $3p$ ionization.

Finally, the electron emission associated with these projectile energy losses must be corrected for electric-field effects which influence the relative number of ejected electrons of a particular energy that are detected. SIMION simulations as described below were used to provide this information. This results in an "effective" ejected electron energy that is smaller than the mean projectile energy loss. The ejected energy profiles are shown by the symbols with their average energies and limits for 3/4 of the total intensity listed. Henceforth,

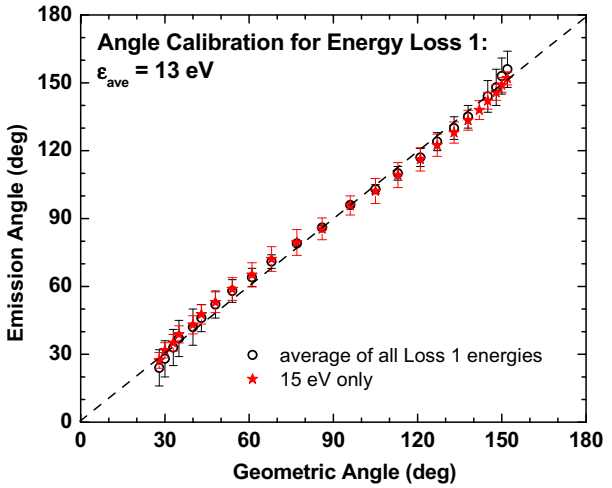

FIG. 3. Angular calibration for the loss 1 energy-loss window comparing a weighted average of all ejected electron energies with the calibration for only 15-eV electrons. The dashed curve represents a one-to-one correspondence between the observed geometric angle and the emission angle.

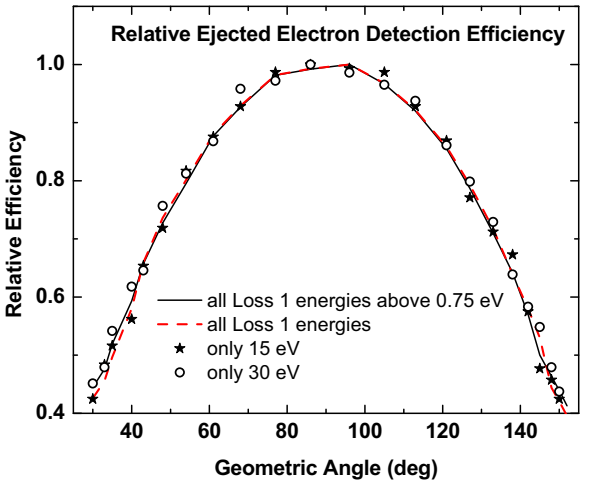

FIG. 5. Relative ejected electron detector efficiency as a function of the geometric angle, and energy losses. The solid curve considers only ejected electron energies above 0.75 eV, which neglects the turned around electrons; the dashed curve considers an average of all ejected electron energies; solid stars (hollow circles) consider only ejected energies of 15 and 30 eV.

for the lower electron emission case (loss 1) an average value of 13 ± 8 eV will be used. Due to the higher energies, electric-field effects are minimal for loss 2 where the ejected electron energies are 26 ± 10 eV.

2. *Ejected electron angular calibration*

As stated earlier, when these data were first collected the extended interaction volume, and possible modifications of ejected electron trajectories by the electric field, used to extract recoil ions inhibited conversion of our measured yields to relative cross sections as functions of ejection angles and energies. A computer model was developed to convolute theory with our experimental conditions but attempted deconvolutions of the data were unsatisfactory. However, recently [20] by using detailed SIMION simulations good agreement between our measured data for electron impact on N_2 with published data was shown.

Using the same procedure, the angular calibration for the ejected electrons was performed by using the SIMION code in which 13 emission energies were considered (0.5, 1, 2, 3, 5, 10, 15, 20, 30, 40, 50, 60, and 70 eV) for electrons emitted towards the detector (angle between 0 and 180°) and two energies were considered (0.5 and 1 eV) for electrons emitted away from the detector (angle between 180 and 360°), but which are turned around because of the electric fields present in the interaction region. Simulations were performed for about 50 000 particles originated in a volume equivalent to the superposition of the beam and the gas jet target, considering the target density as well. These data were sorted into bins just as for the experimental data. This provided an angular calibration

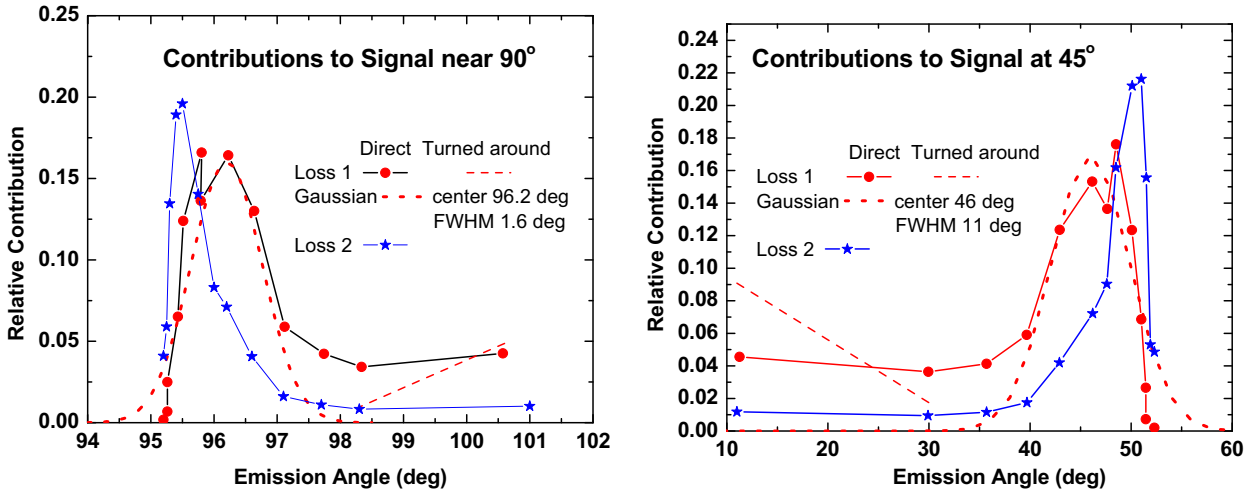

FIG. 4. Relative contribution of emitted electrons according to their trajectories: directly towards the detector (curves with solid points) or turned around (dashed curves), for events near 90° (left) and 45° (right) for "effective" ejected energies of 13 eV (red) and 26 eV (blue). A Gaussian fit is added (dotted curve) as a guide to the reader for 13-eV data.

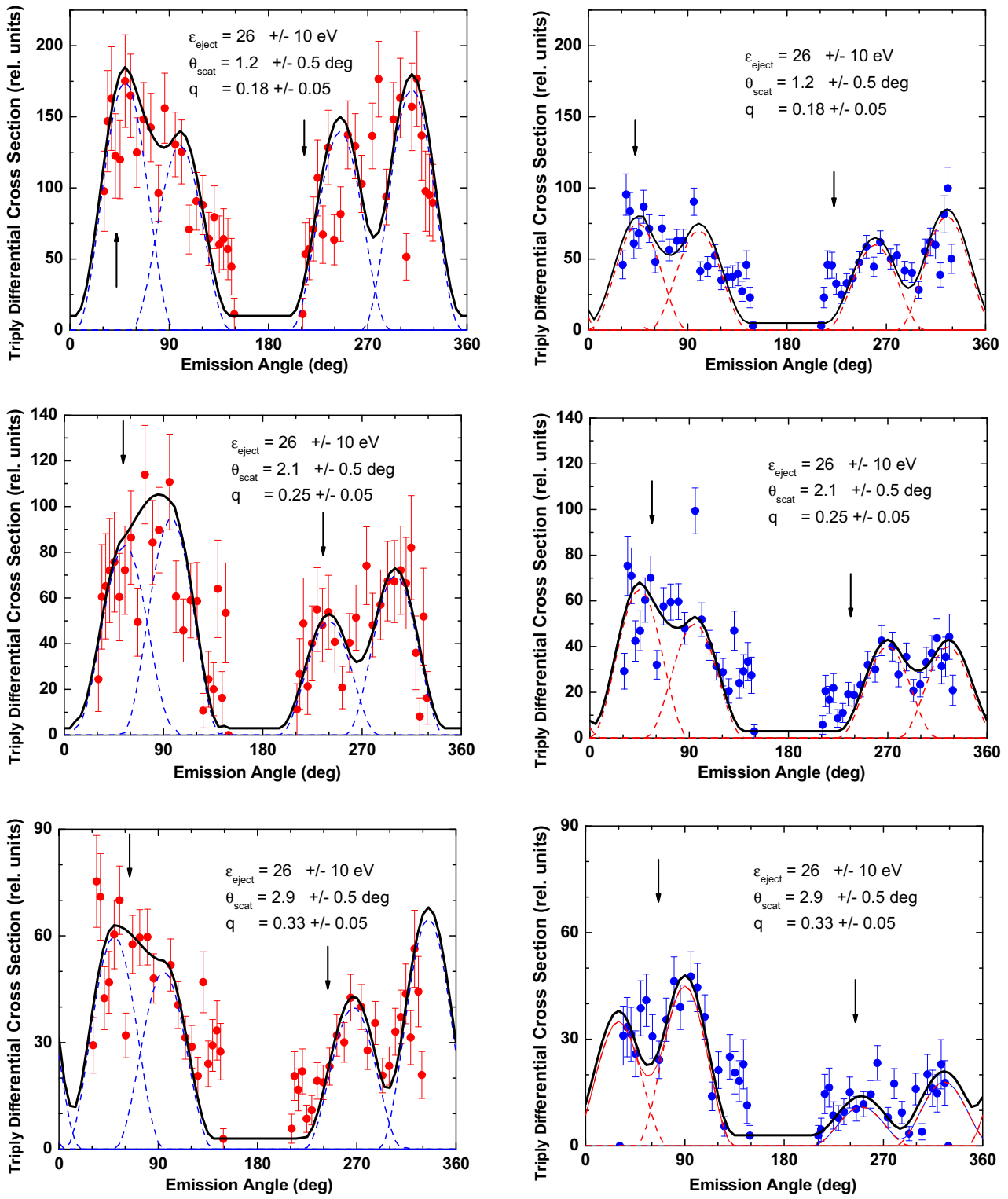

FIG. 6. TDCS results as a function of the scattering and emission angle for average ejected electron energies of 26 eV for single ionization of Ar, induced by positron (left) or electron (right) impact. The solid and dashed lines are visual fits to the data as described in the text.

which describes both the actual emission angle and the relative detection efficiency as a function of the geometric angle (see Fig. 1). The reader should note that these calibrations are often done by comparing measured results with known angular distributions and cross sections or with isotropic features such as Auger emission. Unfortunately, data for our experimental parameters, particularly for positron beams, do not exist and Auger type measurements are impossible for our beam intensities.

An example of the results for the angular calibration is shown in Fig. 3. The calibration was tested by following two procedures: first a full analysis was performed, simulated

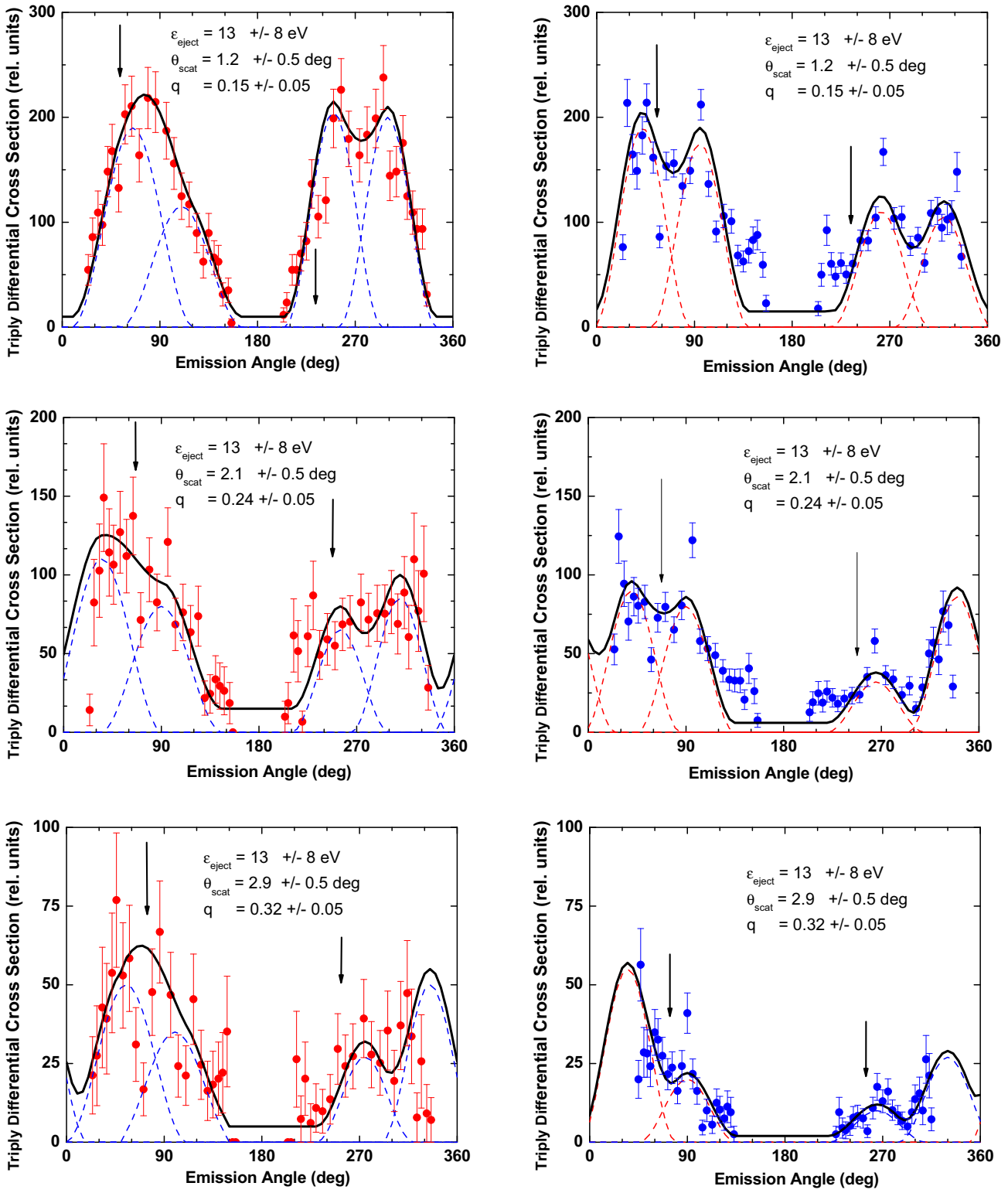

FIG. 7. TDCS results as a function of the scattering and emission angle for average ejected electron energy 13 eV for single ionization of Ar, induced by positron (left) or electron (right) impact. As in the previous figure, the dashed and solid curves are visual fits to the data.

results were sorted, and data for each emission energy were weighted to account for its relative contribution and summed (for further details see the energy-loss calibration procedure). In contrast, the same information was generated by using only the "nominal" emission energy. From the figure it is clear that both procedures result in identical, within error bars, angular calibrations. Finally, an angular calibration curve was then generated for each one of the energy losses employed.

TABLE I. Parameters used for visual fits to data shown in Figs. 5 and 6. The width parameter w was 2 except for the positron impact loss 1 binary peaks where a value of 1.6 was used.

Electron	q (a.u.)	$Qang$ (deg)	B	A bin 1	θ_{max}bin 1	A bin 2	θ_{max}bin 2	A rec 1	θ_{max}rec 1	A rec 2	θ_{max}rec 2
Loss 1 2.9 deg	0.32	73	2	55	35	20	90	10	265	27	330
Loss 1 2.1 deg	0.24	67	6	90	40	80	90	32	265	86	340
Loss 1 1.2 deg	0.15	55	15	190	42	175	95	110	262	105	320
Loss 2 2.9 deg	0.33	66	3	35	30	45	90	11	250	18	325
Loss 2 2.1 deg	0.25	59	3	65	45	50	95	40	270	40	325
Loss 2 1.2 deg	0.18	44	2	75	45	70	100	60	260	80	325
Positron											
Loss 1 2.9 deg	0.32	73	5	50	55	35	100	27	275	50	335
Loss 1 2.1 deg	0.24	67	15	110	35	80	90	65	255	85	310
Loss 1 1.2 deg	0.15	55	10	190	65	115	110	205	250	200	300
Loss 2 2.9 deg	0.33	66	3	60	50	50	95	40	267	65	335
Loss 2 2.1 deg	0.25	59	3	80	55	95	97	50	240	70	300
Loss 2 1.2 deg	0.18	44	10	175	50	130	100	140	245	170	310

3. *Ejected electron angular detector efficiency calibration*

The relative detector efficiency was calculated from the SIMION simulations as well. In this case SIMION sorted results were used to estimate the contribution of each emission energy at each observation angle. Results showed that small energies (<1 eV) are concentrated in the region near the center (near 90°), and turned around low-energy electrons are significant only at the extreme angles (near 45 or 135°). A closer look is shown in Fig. 4 where the relative contribution of each emission energy, e.g., 0.5, 1, 2, . . . , 70 eV, is plotted as a function of emission angle. The near 90° curves are for increasing energies from right to left while at 45° the energy is increasing from left to right. The dashed curves are for 0.5− and 1-eV emission that is turned around by the electric field. Because of the electric field and binning, each emission energy gives a specific average emission angle. It can be seen that energies around the mean energy dominate and lead to a narrow range of emission angles, while low-energy and turned around electrons contribute less than 20% for a "nominal" emission energy of 13 eV and practically nothing for a "nominal" energy of 26 eV. The dotted curves are Gaussian fits to the broader distributions for the lower-energy data. With this information the SIMION data allowed us to calibrate the ejected electron detection efficiency as a function of the geometric angle of observation. As seen in Fig. 5, the detection efficiencies at each emission angle bin are virtually identical whether either a weighted average of all energies, or where low-energy and turned around electrons are ignored, or simply the weighted mean of emission energies is used.

B. TDCS results

This calibration procedure was used to generate the TDCS from the measured coincidence data. The results are shown in Figs. 6 and 7. From the figures it is possible to distinguish two interaction regions in terms of the emission angle (θ_e), as defined before: binary ($0° < \theta_e < 180°$) and recoil ($180° < \theta_e < 360°$). As in similar previous measurements for electron impact ionization [1–3], we can notice that binary interactions appear to be composed of two peaks, located around 45° and between 90 and 120°; for recoil interactions, again two peaks are present, located near 270° and between 300 and 330°. Dashed curves are visual fits to each peak using the following fitting function:

$$A\cos^2[w(\theta_{max} - \theta_e)] \quad (1)$$

where A corresponds to the maximum amplitude of the peak centered at θ_{max} and w is the peak width used as a parameter to narrow the cosine square curve. Solid curves correspond to the sum of fitted peaks and background. As stated, these are visual fits and are only meant to provide a guide to the eye. However, to aid the interested reader, values for the curve parameters are listed in Table I. There is also a hint of a third peak around 180°, but due to the lack of data it is not possible to accurately determine its existence. The overall fit spectrum is then composed of the sum of the individual peaks plus a constant background B.

In a further examination of the TDCS data, our visual fits imply that for electron impact the first binary peak is shifted toward the forward direction with respect to the momentum-transfer direction with the shift increasing with increasing momentum transfer. For positron impact, the first binary peak is shifted away from the forward direction for small momentum transfer but systematically rotates toward a shift in the forward direction. The recoil interactions show that the first peak is always more forward directed with respect to the **–q** vector. For electron impact both recoil peaks are always in directions approximately 225° from their respective binary peaks while for positron impact the difference in directions systematically increases from approximately 180 to 230°.

The relative intensity between binary and recoil interactions has been an interesting subject, mainly because it depends strongly on the theoretical approach used to calculate it. By considering the contribution of both peaks in the binary and recoil regions it is possible to calculate their total intensities which exhibit an exponential decay as a function of momentum transfer, as can be seen in Fig. 8. The main highlights of this calculation are that the recoil intensity tends to be larger than the binary intensity for positron impact but is smaller for electron impact and both the binary and recoil intensities are bigger for positron impact, in contrast to theoretical predications which imply the recoil intensity should be larger for electron impact.

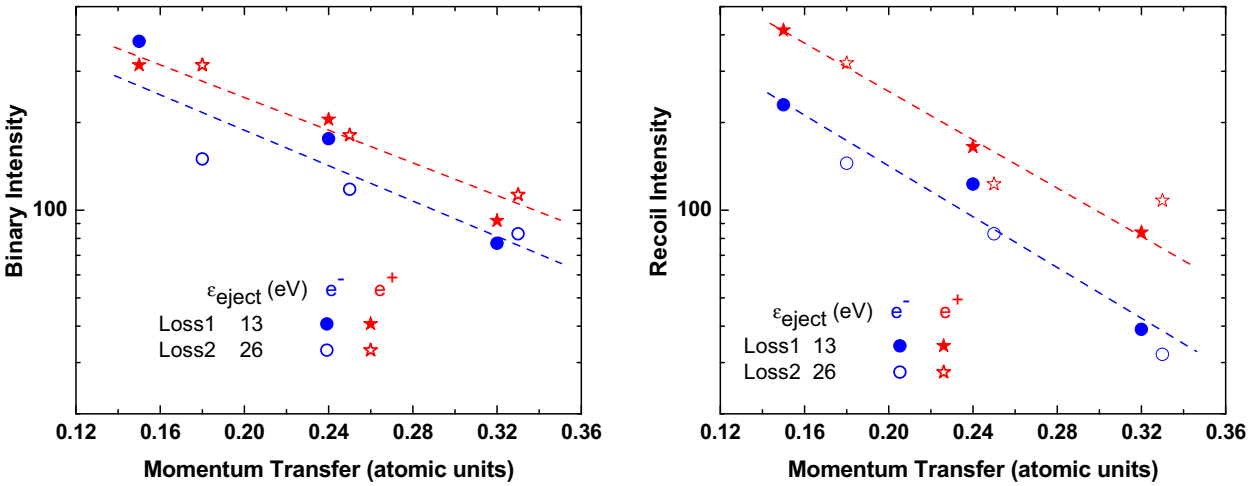

FIG. 8. Relative intensity of binary interactions (left) and recoil interactions (right) for positron impact (red) and electron impact (blue), as a function of momentum transfer. Solid and hollow points correspond to average ejected electron energies of 13 and 26 eV.

IV. REMARKS

Fully differential ionization of argon has been presented for both positron and electron impact. The influence of different experimental parameters on the raw data has been described. Detailed simulations of the trajectories for the ejected electrons were used to obtain a detailed calibration of the ejected electron emission angle and detection efficiency and for the projectile energy loss, thus providing TDCS information as a function of the momentum transferred in the collision process. In accordance with previous TDCS studies for electron impact, both the binary and recoil regions were shown to be composed of two peaks. These were visually fitted with a modified cosine squared function. Indications of additional structure around 180° were also seen. As we are not aware of any experimental or theoretical data which can be directly compared to our measurements, we concentrated instead on relative comparisons between positron and electron impact and on extracting trends as a function of momentum transfer. By comparing the positron and electron impact data, differences for binary and recoil interactions, associated with the sign of the projectile charge, were shown. An enhancement on the intensity of binary and recoil interactions for positron impact was noted, when compared to those for electron impact. Such intensities were found to have an exponential decrease as a function of the momentum transfer. By looking at the ejected electron angular distributions, maxima of the peaks associated with the binary and recoil interactions consistently showed a shift with respect to the direction of momentum transfer, thus providing an indication of the influence of postcollision interactions on the collision process.

ACKNOWLEDGMENTS

Data collection and analysis were supported by the NSF and Universidad Nacional Autónoma de México DGAPA-PAPIIT under Contract No. IN-116916.

[1] E. Weigold and I. E. Mccarthy, Adv. At. Mol. Phys. **14**, 127 (1979).
[2] P. J. O. Teubner, in *Electron Impact Ionization*, edited by T. D. Märk and G. H. Dunn (Springer-Verlag, Vienna, 1985), pp. 89–136.
[3] A. Lahmam-Bennani, J. Phys. B **24**, 2401 (1991).
[4] G. Laricchia, S. Brawley, D. A. Cooke, Á. Kövér, D. J. Murtagh and A. I. Williams, J. Phys. Conf. Ser. **194**, 012036 (2009).
[5] S. Sharma and M. K. Srivastava, Phys. Rev. A **38**, 1083 (1988).
[6] M. Brauner and J. S. Briggs, J. Phys. B **26**, 2451 (1993).
[7] J. Berakdar, J. S. Briggs, and H. Klar, J. Phys. B **26**, 285 (1993).
[8] Á. Benedek and R. I. Campeanu, Nucl. Instrum. Methods B **266**, 458 (2008).
[9] O. G. de Lucio, J. Gavin, and R. D. DuBois, Phys. Rev. Lett. **97**, 243201 (2006).
[10] R. D. DuBois, O. G. de Lucio, and J. Gavin, Europhys. Lett. **89**, 23001 (2010).
[11] O. G. de Lucio, S. Otranto, R. E. Olson, and R. D. DuBois, Phys. Rev. Lett. **104**, 163201 (2010).
[12] G. Gabrielse, Adv. At. Mol. Opt. Phys. **50**, 155 (2005).
[13] B. Feng, H. C. Glifford, R. D. Beach, G. Boening, M. A. Gennert, and M. A. King, IEEE Trans. Med. Imaging **25**, 838 (2006).
[14] B. J. Fueger *et al.*, Molecular Imaging and Biology **11**, 269 (2009).
[15] C. Champion and C. Le Loirec, Phys. Med. Biol. **51**, 1707 (2006).
[16] A. P. Mills, Jr., in *Positron Solid State Physics*, edited by A. Dupasquier and W. Brandt (North-Holland, Amsterdam, 1983), p. 734.
[17] A. P. Mills, Jr., in *Positron Spectroscopy of Solids*, edited by A. Dupasquier and A. P. Mills, Jr. (IOS, Amsterdam, 1995), p. 805.
[18] P. J. Schultz and K. G. Lynn, Rev. Mod. Phys. **60**, 701 (1988).
[19] G. Laricchia *et al.*, Radiat. Phys. Chem. **68**, 21 (2003).
[20] O. G. de Lucio and R. D. DuBois, Phys. Rev. A **93**, 032710 (2016).
[21] J. Gavin, Ph.D. thesis, Missouri University of Science and Technology, 2009.